# Electromagnetic Signatures for Drone Detection and Recognition

**Tomas Jačionis[1,*], Šarūnas Mikučionis[1], Vytautas Urbanavičius[1]**
*[1] Department of Electronic Systems, Vilnius Gediminas Technical University,*
*Plytines St. 25–P2 211, LT-10105 Vilnius, Lithuania*
*tomas.jacionis@vilniustech.lt[*]; sarunas.mikucionis@vilniustech.lt;*
*vytautas.urbanavicius@vilniustech.lt*

***Abstract*— Modern unmanned aerial vehicle (UAV) platforms predominantly rely on electric propulsion for controlled flight. Most current UAV propulsion systems employ brushless DC (BLDC) thrust motors. This paper demonstrates the passive detection of UAV electric propulsion systems using a dynamically changing alternating electromagnetic (EM) field created by BLDC thrust motors and power lines in the very low frequency and low frequency range. A high-performance low-noise amplifier and a commercial Airspy HF+ SDR paired with compact ferrite-core magnetic antenna, are used to capture near-field magnetic emissions from four different drones. The tested platforms include the mass-produced DJI Mini 2, DJI Mavic 2 Enterprise, DJI Air 3S, and the Eachine Tyro 109. The measured EM spectrum consistently exhibit motor phase-commutation components and electronic speed controller PWM components with propulsion load-dependent sidebands, enabling extraction of time, frequency, and amplitude-dependent propulsion-related BLDC motor EM signatures for UAV detection and recognition. The experiment results show the capabilities of drone swarm detection and recognition of each propulsion system flight mode.**

***Index Terms*— unmanned aerial vehicles (UAVs); brushless DC (BLDC) motors; thrust-motor electromagnetic (EM) signature; near-field EM detection.**

## I. INTRODUCTION

Unmanned aerial vehicles (UAV) have become widely available and are increasingly observed in both legitimate and malicious scenarios, creating a growing demand for reliable detection around sensitive areas [1]. Among the available sensing modalities, radio-frequency (RF) techniques are particularly attractive because they can be implemented passively, operate day and night, and, in many cases, provide early warning at long ranges. RF-based detection leverages the fact that many UAV systems radiate electromagnetic (EM) energy through their command-and-control links, telemetry channels, video downlinks, and onboard electronics [2]. In principle, monitoring these emissions enables not only detection but also classification (e.g., protocol family, manufacturer, drone position) and sometimes localization of the transmitter [3].

Multirotor drones increasingly operate with strict radio-silence settings, making conventional electronic intelligence and RF direction-finding approaches inefficient [1], [3]. New approach of optical-fiber controlled drones makes drone flights undetectable in radio communication frequency bands and undetectable with up-to-date radio communication counter UAV systems [4], [5].

Yet every electrically powered UAV has a mandatory item, which must be an electric propulsion system, usually based on one or several brushless DC (BLDC) motors. During flight, such propulsion systems create a dynamically changing alternating EM field, the frequency spectrum of which, for brevity, will hereafter be called the EM signature of the UAV. Investigation of multirotor drone propulsion system under different flight modes is presented in this paper. The slightest air movement during the drone flight influences operation of drone multiple motor propulsion system. This accordingly changes the execution of the drone's flight stabilization algorithms, which control the individual propulsion of each BLDC thrust motor. The inflight drone rotations on each axis have a recognizable multimotored propulsion change with observed EM emissions in the frequency spectrum [6]. The received EM emission spectrum change consistently exhibit motor phase-commutation components and electronic speed controller (ESC) pulse-width modulation (PWM) components with propulsion load-dependent sidebands [7], enabling extraction of time, frequency, and amplitude-dependent propulsion-related BLDC motor signatures for UAV detection and recognition. Receiving and interpreting these very low and low frequency (VLF and LF) EM signatures offers a passive, covert, and legally simpler way of situational awareness in airspace where other sensing modalities underperform.

Practical detection and characterization of BLDC thrust-motor EM signatures are analysed in this paper. Airspy HF+ software-defined radio (SDR), compact ferrite loop antennas optimized for strong magnetic-field coupling and electric-field rejection in the VLF and LF spectrum covered by the SDR receiver were used for detection. This paper presents a controlled and comparative measurements on serial production drone platforms spanning consumer, enterprise, and DIY categories: DJI Mini 2, DJI Mavic 2 Enterprise, DJI Air 3S, and Eachine Tyro 109. Across EM emissions from drone electric thrust system occurring at hover, climb, descent, and other manoeuvres, generate time and frequency dependent EM signatures enabling identification of each drone separately, even in the drone swarm conditions.

This paper provides a research gap in RF-based UAV detection. Most of the recent research papers on the topic

focus on the reception of radio communication signals and the decoding of encrypted data, where the detectable source is assumed to be the communication link between the UAV and its operator. Such systems intercept control, telemetry, video, Wi-Fi-like, Bluetooth-like, or Drone ID signals and then apply spectrum analysis, protocol decoding, or machine-learning classification. This approach is only effective when the UAV is not working in complete radio silence or under fibre-optical cable control. A key novelty of the present study is the direct association between measured VLF/LF EM signatures and propulsion-control mechanisms. The observed spectra contain PWM switching components, motor phase commutation-related sidebands, and load-dependent harmonic-amplitude variations. These features constantly change during take-off, hover, vertical acceleration, yaw rotation, and stabilised flight, because the flight ESC controller continuously modifies individual motor thrust to maintain attitude and trajectory. Consequently, the EM signature contains not only information about UAV presence, but also information about propulsion state and flight mode dynamics.

The novelty of this work lies in defining and experimentally validating a propulsion-based electromagnetic signature for UAV detection and recognition, explaining the origin of the EM signature forming.

The closest to the topic of EM based UAV detection is the study of Blažek et al. [14], which demonstrated that small UAV BLDC motors and ESCs generate measurable magnetic field. This study did not cover a complete propulsion signature interpretation for modern commercial UAV platforms, flight mode dependent spectral behaviour, or simultaneous multi UAV recognition. The present work extends that earlier foundation by experimentally measuring EM emission of serial-production UAVs, demonstrating that each tested UAV platform exhibits a characteristic propulsion-related EM signature centred on its ESC PWM switching frequency, with information related to the UAV's flight.

The remainder of the paper is organised as follows. The second, theoretical part examines the main sources of EM radiation from the drone's propulsion system, presents a mathematical model of the system of wires that power the drone's BLDS motors, and simulates the distribution of the magnetic field they generate. The third section is experimental and the most extensive; it briefly presents the objects of study (drones), the experimental setup and equipment used, and the results of measuring the drones' EM signatures at various distances. The fourth part discusses the obtained measurement results and draws conclusions about the possibility of detecting and recognising drones based on the EM emissions of their propulsion system. The paper ends with a brief summary.

## II. TECHNICAL AND THEORETICAL JUSTIFICATION

### *A. Electromagnetic Signature Generating Devices*

Every electrically powered drone has devices which are mandatory for the flight performance. Fixed wing, helicopter or multicopter electrically powered UAVs must have one or several BLDC thrust motors to perform the flight as a mandatory device. The thrust control of BLDC the motors is implemented in a similar manner, where the PWM duty cycles are defined by physical characteristics, well known and characterised [8]. The ESC used to control the thrust of the BLDC motor does have its phase commutation and PWM switching frequency. Three BLDC motor phase coils are switched proportionally to the BLDC motor rotation change and PWM duty cycle, while PWM switching frequency is constant and programmable [9]. Quadcopters examined in this paper are of the serial production defined in the Fig. 1.

The three main components of EM emission in VLF and LF range are examined in this paper, which are influenced by: 1st – BLDC motor phase commutation frequency (always proportional to BLDC motor rotation, acceleration and deceleration), 2nd – PWM duty cycle, which is proportional to the BLDC motor rotation, acceleration, deceleration, and 3rd – PWM switching frequency, which is constant and can be changed in ESC microcontroller settings. All these EM emissions occur in VLF and LF range described by ITU designation [10], in the frequency range of 3–30 kHz and 30–300 kHz, or wavelength ranges from 100 to 10 km and from 10 to 1 km respectively [11].

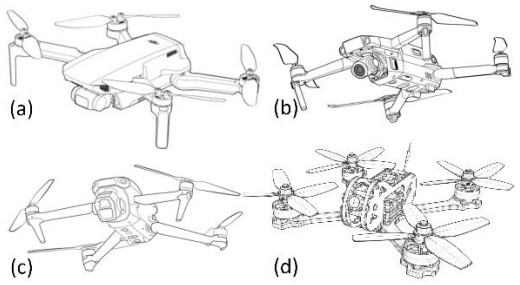


Fig. 1. BLDC thrust motor powered serial production drones used in the experiment for EM signature detection test; where (a) drone is DJI Mini 2, (b) is DJI Mavic 2 Enterprise, (c) is DJI Air 3S, and (d) is Eachine Tyro 109.

The highest current devices found in electrically powered multicopters are the electric thrust motors. In the quadcopter drone, four BLDC thrust motors are used. Each of them must have a separate ESC for the thrust control [12]. There are two most common connection types of the quadcopter drone propulsion systems presented in Fig. 2 (a) and (b). The main difference is in the ESC type, a single board ESC is used to power all four BLDC thrust motors (Fig. 2 (a)), and four separate ESCs are used to power four BLDC thrust motors (Fig. 2 (b)). It is important to note that BLDC motors are not only powered from the power supply, but also generate back EMF, which is sent back to the ESC.

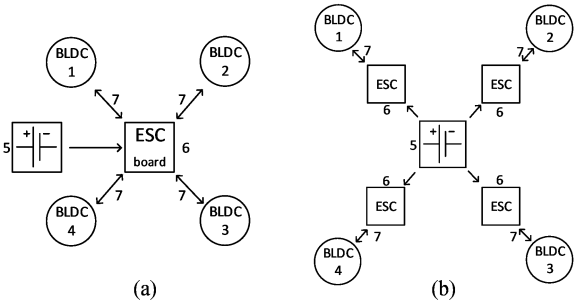


Fig. 2. Block diagram of quadcopter highest current components, which form the EM signature: single ESC board (a) and multiple ESC boards (b); where 1, 2, 3, 4 are BLDC thrust motors with three wire cable system

connected to the ESC, 5 is power supply battery, 6 is ESC module and 7 are the BLDC thrust motor connecting wires.

The highest power EM emissions are produced by the highest alternating currents, originating in the battery leads, ESC and BLDC [13]. The current between the battery and ESC is DC, and the current between the ESC and BLDC thrust motor is AC with known frequency and EM emission signature [14]. Each ESC is connected to a BLDC thrust motor using three wires (Fig. 3), which are usually not shielded and emit EM energy, the signature of which can be detected. The motor wire length is directly proportional to the multicopter lifting capacity, as the longer propellers have a bigger distance in between [15]. The higher the multicopter weight and lifting capacity, the higher AC currents tend to flow in the wires between ESC and BLDC motor [12], [16]. The mechanism of EM energy radiation from drone BLDC motors is presented in more detail in Appendix A.

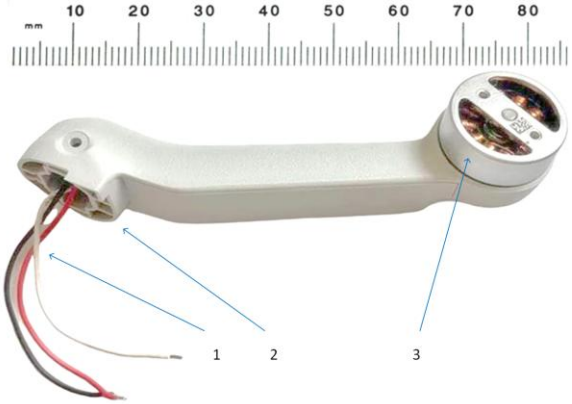


Fig. 3. DJI Mini 2 quadcopter BLDC thrust motor mounting arm; where 1 are three coil power cables, 2 is thrust motor foldable mounting arm, 3 is BLDC thrust motor rotor.

### *B. Mathematical Model of Magnetic Field Emitted by the Propulsion System of a Quadcopter*

Most commercially produced UAVs use four electric motors arranged in a cross pattern as thrust motors (Fig. 1) [17]. UAVs of this design are commonly called *quadcopters* [18].

Alternating currents flowing through the wires from the quadcopter ESC to the traction electric motors emit EM energy which can be detected by modern electronic devices. Since the frequency of the power supply currents of quadcopters is within tens, and rarely hundreds, of kilohertz [19], then in order to detect a quadcopter, it is necessary to receive only the magnetic component of this radiation; in this case, the antenna of the quadcopter detection receiver can be of feasible dimensions (especially when using ferrite cores).

To simplify the study of the magnetic field emitted by the quadcopter's propulsion system, its motor system can be represented as two crossed Hertzian (electric) dipoles. Such a system of dipoles, which are fed by currents of the same amplitude, but shifted in phase by 90˚, is widely known as a "turnstile elementary emitter" [20], [21]. However, it seems natural to assume that the currents of the quadcopter thrust motors during flight can differ in many parameters – amplitude, phase shift, frequency, etc. The proposed model assumes that the quadcopter motors, located on opposite arms, are powered by currents of the same parameters, and compared to neighbouring motors, the currents may differ in amplitude, and the phase shift may also be arbitrary.

The relevance of analysing magnetic, rather than electric, field strength is based on the fact that in the case of VLF (super long waves), it is technically simpler to design antennas sensitive to magnetic fields; such antennas are sometimes even called magnetic field sensors. The directivity characteristics of antennas are usually calculated and measured in the far zone, but there are cases when the magnetic or electric field intensity needs to be determined in the near zone, where the distance from the stopping point to the radiator is less than half of the wavelength (in the case of a quadcopter, with a frequency of about 100 kHz, the wavelength is 3 km, and this is already a fairly large distance). Taking into account the above facts, it was decided to create a mathematical model of the magnetic field created by crossed Hertzian dipoles, allowing calculating the magnetic field intensity at any observation point and under different dipole excitation conditions.

### *C. Quadcopter Propulsion System Magnetic Field Model Equations*

To create a simplified mathematical model of the magnetic field emitted by the quadcopter motor system, the crossed Hertzian dipoles are placed at the centre of the coordinate system so that the *z* axis is perpendicular to the plane of the dipoles (Fig. 4). One of the dipoles coincides with the *x*-axis, and the other with the *y*-axis.

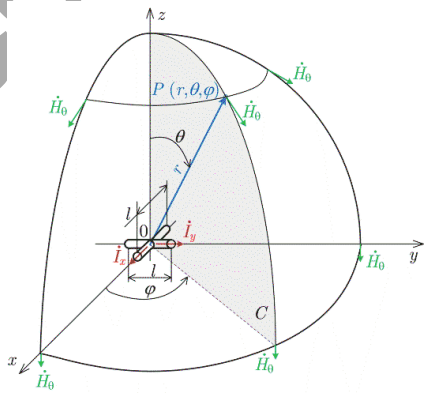


Fig. 4. Crossed dipoles in a spherical coordinate system.

In order to determine the influence of current amplitudes and phase differences on the magnetic field intensity, let us assume that

$$\dot{I}_x = I_x \, \mathrm{e}^{\mathrm{j}\varphi_x}, \quad \dot{I}_y = aI_x \, \mathrm{e}^{\mathrm{j}(\varphi_x + b\pi/2)}; \tag{1}$$

where $\dot{I}_x$ and $\dot{I}_y$ are the complex amplitudes of the currents of the corresponding dipoles, $\varphi_x$ is the initial phase of the current flowing in the *x* dipole, $0 \le a \le 1$ is a coefficient that allows changing the ratio of the amplitudes of the currents in the dipoles, and $0 \le b \le 2$ is a coefficient that allows us to change the phase difference of the currents; when *a* and *b* are equal to 1 then the crossed dipoles correspond to the turnstile radiator. For simplicity, let it is assumed that the initial phase of the current $I_x$ is zero. Thus, the currents are expressed as:

$$\dot{I}_x = I_x, \quad \dot{I}_y = aI_x \, \mathrm{e}^{\mathrm{j}(\pi/2)b}. \tag{2}$$

The amplitude of the magnetic field created by crossed dipoles is calculated as follows:

$$H(r,\theta,\varphi)=I_x\frac{l}{4\pi r^2}\sqrt{1+(\beta r)^2}\cdot\sqrt{d_\theta^2+d_\varphi^2\cos^2\theta}\,; \quad (3)$$

where

$$d_\theta^2=\left[\sin\varphi-a\cos\varphi\cos\left(\frac{b\pi}{2}\right)\right]^2+\left[a\cos\varphi\sin\left(\frac{b\pi}{2}\right)\right]^2 \quad (4)$$

is the coefficient of the difference in the excitation currents of the meridian component of the magnetic field;

$$d_\varphi^2=\left[\cos\varphi-a\sin\varphi\cos\left(\frac{b\pi}{2}\right)\right]^2+\left[a\sin\varphi\sin\left(\frac{b\pi}{2}\right)\right]^2 \quad (5)$$

is the coefficient of the difference in the excitation currents of the azimuthal component of the magnetic field; $l$ is the length of the dipole; $r$ is the distance from the centre of the crossed dipoles to the point of observation; $\theta$ and $\varphi$ are correspondently the meridional the azimuthal angles of the spherical coordinate system; $\beta=2\pi/\lambda$ is the phase coefficient; $\lambda$ is the length of the electromagnetic wave emitted by the quadcopter motor system.

### *D. Computer Calculation of the Magnetic Field of the Quadcopter Propulsion System*

In order to determine the dependence of the magnetic induction induced by the quadcopter's propulsion system on the observation point and the quadcopter's position, a script was written, and simulation calculations were performed using equation (3) in MatLab®. The quadcopter propulsion system was simulated by two crossed dipoles 0.3 m long, with a maximum amplitude of the motor supply currents taken to be 20 A at a frequency of 30 kHz; the distance from the dipoles to the observation (induction calculation) point was chosen to be 100 meters. It was assumed that during the flight of the quadcopter, the phase difference of the supply currents can vary within the range from 0 to π/2, and their amplitudes – from 5 A to 20 A. The calculation results are presented in the form of radiation patterns in Fig. 5 to Fig. 7 and in the Tables I–III. The dashed red line on all figures for comparison shows the radiation pattern of an elementary turnstile emitter.

In the first simulation, it was assumed that the quadcopter flies in a stationary mode, the amplitudes of the supply currents are equal $I_x = I_y = 20$ A, and the phase shift between the currents is zero (Fig. 5, Table I).

It can be seen in Fig. 5 (a) that at equal motor currents the quadcopter's propulsion system does not radiate in the azimuthal plane at $\varphi = 45^\circ$ and $\varphi = 225^\circ$. However, in the vertical plane, at $\varphi = 135^\circ$ and $\varphi = 315^\circ$ (Fig. 5 (b)), the quadcopter emits EM energy uniformly in all directions except for the angles $\varphi = 45^\circ$ and $\theta = 90^\circ$, in the direction of which the radiation is zero Fig. 5 (c).

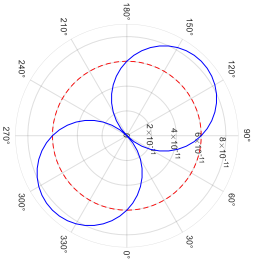

(a)

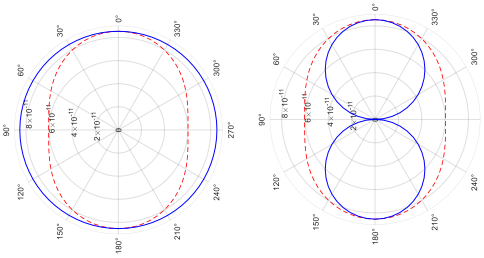

(b) (c)

Fig. 5. Calculated radiation pattern of the quadcopter thrust system in the azimuthal plane (a) and in the meridian plane with the angle $\varphi = 135^\circ$ (b) and $\varphi = 45^\circ$ (c), with the same amplitudes of the supply currents $I_x = I_y = 20$ A and phase difference between the currents of 0.

TABLE I. DEPENDENCE OF MAGNETIC INDUCTION $B$ ON THE MERIDIAN ANGLE $\theta$ WITH THE SAME AMPLITUDES OF THE SUPPLY CURRENTS $I_x = I_y = 20$ A AND A PHASE SHIFT BETWEEN THEM $\Delta\psi = 0$.

| $\theta$ | 0 | 30° | 45° | 60° | 90° |
|---|---|---|---|---|---|
| $B^*$[pT] | 85.318 | 85.318 | 79.807 | 85.318 | 85.318 |
| $B^{**}$[pT] | 85.318 | 73.877 | 60.329 | 42.659 | 0 |

* This value of magnetic induction corresponds to the angle $\varphi = 135^\circ$;
** This value of magnetic induction corresponds to the angle $\varphi = 45^\circ$;

In the second case, the quadcopter is simulated to perform a certain manoeuvre, while the amplitude of current $I_x$ = 20 A, and the amplitude of current $I_y$ = 5 A, the phase shift between the currents is zero (Fig. 6, Table II).

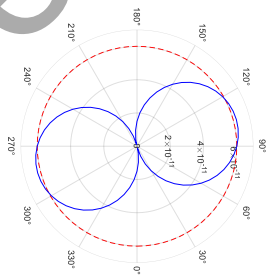

(a)

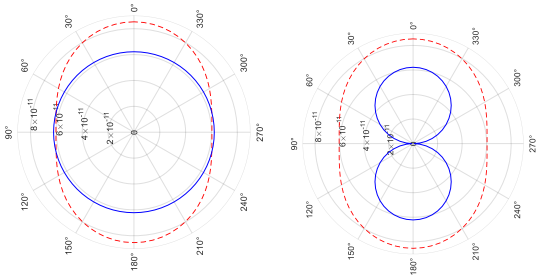

(b) (c)

Fig. 6. Calculated radiation pattern of the quadcopter thrust system in the azimuthal plane (a) and the meridian plane with the angle $\varphi = 105^\circ$ (b) and $\varphi = 15^\circ$ (c), with amplitudes of the supply currents $I_x = 20$ A and $I_y = 5$ A and phase difference between the currents of 0.

TABLE II. DEPENDENCE OF MAGNETIC INDUCTION $B$ ON THE MERIDIAN ANGLE $\theta$ WITH AMPLITUDES OF THE SUPPLY CURRENTS $I_x = 20$ A AND $I_y = 5$ A AND A PHASE SHIFT BETWEEN CURRENTS $\Delta\psi = 0$.

| $\theta$ | 0 | 30° | 45° | 60° | 90° |
|---|---|---|---|---|---|
| $B^*$[pT] | 62.185 | 62.183 | 62.181 | 62.179 | 62.177 |
| $B^{**}$[pT] | 62.185 | 53.857 | 43.978 | 31.106 | 0 |

* This value of magnetic induction corresponds to the angle $\varphi = 105^\circ$;
** This value of magnetic induction corresponds to the angle $\varphi = 15^\circ$;

It can be seen in Fig. 6 (a) that the quadcopter does not emit in the azimuthal plane at $\varphi = 15^\circ$ and $\varphi = 195^\circ$. However, in the vertical plane, at $\varphi = 120^\circ$ and $\varphi = 300^\circ$, the quadcopter emits EM emission uniformly in all directions (Fig. 6 (b)), however, compared to "stable flight" (Fig. 5 (a)), when the

currents were the same, the radiation intensity is reduced by about 27%. Moreover, in some directions the radiation of a quadcopter slightly exceeds the radiation of an elementary turnstile emitter (Fig. 6 (b), $\theta = 90^\circ$), and in some directions it is less (Fig. 6 (b), $\theta = 0$). In the meridian plane, at an azimuth angle of $\varphi = 15^\circ$, there is no radiation at all at an angle of $\theta = 90^\circ$ (Fig. 6 (c)).

In the third case, it is assumed that the quadcopter performs a different maneuver in which the amplitudes of the supply currents are equal $I_x = I_y = 20$ A, and the phase shift between them is $\pi/4$ (Fig. 7, Table III).

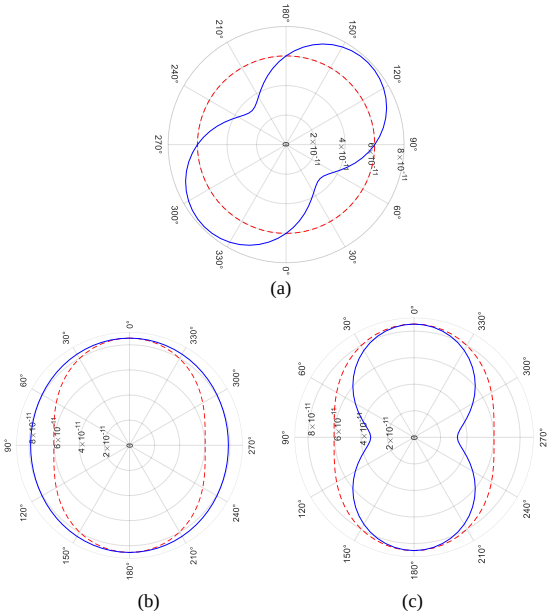

(a) (b) (c)

Fig. 7. Calculated radiation pattern of the quadcopter thrust system in the azimuthal plane (a) and the meridian plane with the angle $\varphi = 135^\circ$ (b) and $\varphi = 45^\circ$ (c), with the same amplitudes of the supply currents $I_x = I_y = 20$ A and phase difference between the currents of $\pi/4$.

TABLE III. DEPENDENCE OF MAGNETIC INDUCTION $B$ ON THE MERIDIAN ANGLE $\theta$ WITH THE SAME AMPLITUDES OF THE SUPPLY CURRENTS $I_x = I_y = 20$ A AND A PHASE SHIFT BETWEEN CURRENTS $\Delta\psi = \pi/4$.

| $\theta$ | 0 | 30° | 45° | 60° | 90° |
|---|---|---|---|---|---|
| $B^*$[pT] | 85.318 | 83.741 | 82.135 | 80.496 | 78.823 |
| $B^{**}$[pT] | 85.318 | 75.669 | 64.595 | 51.179 | 32.650 |

* This value of magnetic induction corresponds to the angle $\varphi = 135^\circ$;
** This value of magnetic induction corresponds to the angle $\varphi = 45^\circ$;

It can be seen in Fig. 7 (a) that the quadcopter in the azimuthal plane at $\varphi = 45^\circ$ and $\varphi = 225^\circ$ radiates less intensely, however, at $\varphi = 135^\circ$ and $315^\circ$, the intensity of its radiation exceeds the intensity of an elementary turnstile emitter of the same dimensions and at the same current amplitudes. However, in the vertical plane (Fig. 7 (b)), at $\varphi = 135^\circ$ and $\varphi = 315^\circ$, the quadcopter emits EM emission almost uniformly in all directions. Moreover, in some directions the radiation of a quadcopter exceeds the radiation of an elementary turnstile emitter, and in some directions it is less (Fig. 7 (c)).

The simulations performed showed that the quadcopter propulsion system, for certain combinations of current amplitudes supplying the electric motors and at zero phase difference between the currents, may not emit any EM energy at all in certain directions (however, in very narrow spatial sectors). However, a quadcopter flying under real conditions almost constantly maintains flight stabilisation mode, responding to external factors and executing specified manoeuvres. In this case, there is a continuous and rapid change in the amplitudes of the currents and the phase difference between them. This assumes a practically uniform radiation of EM energy in all directions, i.e. the shape of the radiation pattern of the quadcopter propulsion system is close to a sphere, which is constantly being slightly compressed from the sides and then immediately returns to its original shape then compresses again, etc.

Calculations made assuming supply current amplitudes of about 20 A show that at a distance of 100 m from the quadcopter the magnitude of magnetic induction can reach 85 pT (Table I and Table II). If we use a hypothetical ferrite antenna with a core diameter of $d = 10$ mm, its relative magnetic permeability $\mu_r = 100$ and the number of coil turns $N = 100$, then in accordance with elementary calculations based on Faraday's law of electromagnetic induction

$$V_m = \frac{d^2}{4}\mu_r B_m N \pi^2 f \qquad (6)$$

with the amplitude of the mentioned magnetic induction of $B_m = 85$ pT, frequency $f = 30$ kHz, an emf with an amplitude $V_m$ of several microvolts will be induced at the terminals of such an antenna. This emf is several times higher than the sensitivity threshold of modern radio receiving devices which can be used to detect quadcopters or drones with a large number of engines.

## III. OVERVIEW OF THE EXPERIMENT

The primary objective of the experiment is to validate the theoretical assumption that the drone's EM signature can be detected by receiving the magnetic component of the drone's EM emission using a magnetic antenna.

### *A. Experimental Setup and Research Objects*

The experiment of EM signature reception was carried out using four serial production drones. Drones used in the experiment are DJI Mini 2 (two items), DJI Mavic 2 enterprise, DJI Air 3S and Eeachine Tyro 109; their main characteristics are presented in Table IV. The magnetic ferrite stick antenna ~~(the layout for setting up ferrite antennas is shown in Fig. 8)~~ was used for signal reception with low noise amplifier and SDR receiver. For received data analysis a portable computer and SDR receivers' software was used. Each drone was powered at a different distance of magnetic antenna for capturing EM signature data. The underground space was used for VLF spectrum noise rejection and detail EM signature reception. The EM signatures of each separate drone at a time were recorded at middle and largest distance from receiving antenna. Not less than three flights were performed with each UAV, and not less than two different measurements of EM signatures are presented in this paper for each tested UAV. At last, EM signatures of three drones hovering at the same time in space were recorded for proving the EM signature detection capabilities in a drone swarm situation. The simplified block diagram of the experiment is represented in Fig 8.

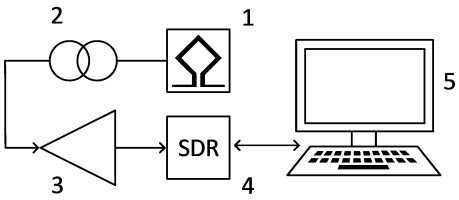


Fig. 8. Experimental equipment set up; where 1 is the magnetic antenna assembly, 2 is the isolating low noise shielded coil, 3 is the low noise regulated signal amplifier, 4 is the SDR receiver, 5 is the control, data collection and analysis computer.

It is important to note that there is little equipment capable of receiving UAV propulsion system EM emissions in the VLF and LF frequency bands in high definition mode. The UAV propulsion related EM emissions could be analysed only due to capture of the received spectrum in high resolution. The Airspy HF+ SDR receiver was chosen among others because of its 9 kHz–31 MHz frequency coverage, high-linearity LNA, 110 dB HF blocking dynamic range, and 22-bit effective resolution in a 3 kHz channel, which is advantageous for resolving narrow PWM switching components, phase commutation sidebands, and harmonic structures.

TABLE IV. MAIN CHARACTERITICS OF INVESTIGATED DRONES.

| Parameter | Drone model | | | |
|---|---|---|---|---|
| | **DJI MINI 2** | **DJI AIR 3S** | **DJI MAVIC 2** | **EACHINE TYRO 109** |
| Drone weight (g) | 249 | 724 | 905 | 411 |
| Battery voltage (V) | 7.7 | 14.6 | 15.4 | 24 |
| Battery capacity (mAh) | 2250 | 4276 | 3850 | 1800 |
| Max speed (km/h) | 57.6 | 75.6 | 72 | 135 |
| Max currents (A) | 15-25 | 25-35 | 20-30 | 18-40 |
| BLDC power bursts (W) | 90-120 | 205-245 | 250-350 | 400-960 |
| Propeller length (cm) | 11.94 × 6.6 | 22.1 × 12.0 | 22.0 × 10.92 | 14.12 × 12 |
| Motor to motor diagonal length (cm) | 22.0 | 42.1 | 40.8 | 22.4 |
| ESC PWM switching frequency (kHz) | 76.8 | 84.2 | 92.5 | 23.9 |

*B. Results of the Experiment*

For validation of the theoretical assumption that the drone's EM signature can be detected by receiving the magnetic component of the drone's EM emission using a magnetic antenna, first of all, the smallest DJI MINI 2 drone was disassembled for electronic measurements. If the smallest drone in a class of lower than 250 grams can be detected, heavier drones will also be detected as more thrust and electric power is necessary, which results in significantly higher currents causing a higher power of the EM signature. DJI Mini 2 drone ESC board was connected to oscilloscope for ESC board PWM frequency measurements. The measured PWM switching frequency of 76.86 kHz was detected, which PWM waveform is represented in Fig. 9.


Fig. 9. DJI Mini 2 PWM switching frequency of ESC at 76.8 kHz at the period of H1-H2.

For the proof of the experimental data, the DJI Mini 2 oscillogram PWM switching frequency was examined with the reception of the EM spectrum using a magnetic stick construction antenna. The obtained EM spectrum with highly expressed drone flight modes was captured for detailed analysis. For the best visualisation, a radio spectrum waterfall (a spectrogram with a 3D data visualization mapping of signal amplitude over both frequency and time) was chosen. In the presented experimental data, for the best EM signature display, time is presented scrolling downwards to show historical activity of the EM signature, frequency increasing from left to right and amplitude with increasing warm colours.

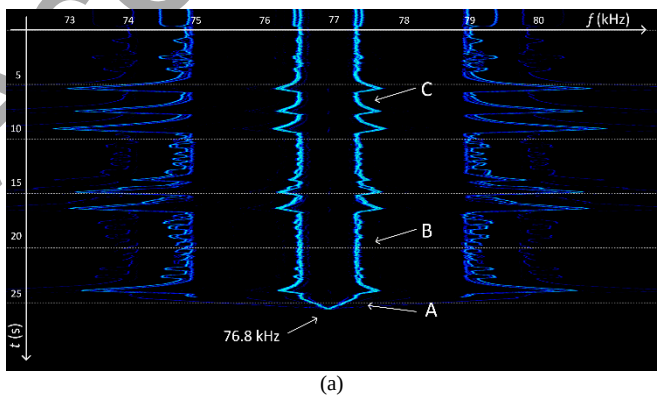


(a)

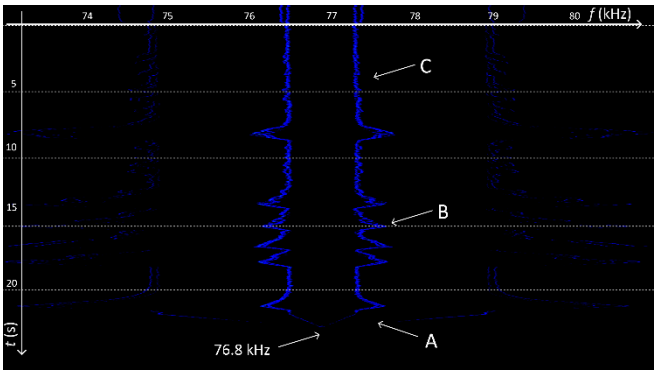


(b)

Fig. 10. DJI Mini 2 drone EM signature at 5-meter distance (a) and at 14-meter (b). The time marks show: A – motors are started; B – drone is in flight stabilisation mode; C – drone is rapidly lifted in vertical axis three times.

The spectrograms in Fig. 10 show the exact same centre PWM switching frequency of 76.86 kHz, which is measured using oscilloscope in the drone ESC BLDC thrust motor power connection wires (Fig. 9). The measured DJI Mini 2 drone PWM switching frequency coincides with the highest

amplitudes centre frequency measured in the EM signatures presented in the Fig. 11, during the spin up procedure of drone folding propellers (spectrogram time mark A). In the Fig. 10 (a) and (b) the DJI Mini 2 drone is lifted at distance of 5 and 14 meters from the receiving antenna. The flight experiment procedure is the same. The EM signature of the drone is of a constant central frequency 76.8 kHz and does not change in the spectrum during all flight modes. Central EM signature frequency coincides with the electronically measured PWM switching frequency. The main difference is the of the amplitude of the visible harmonics and their number. The recorded EM signature of DJI Mini 2 has a difference from other recorded signatures, as it does not have a central frequency signature present.

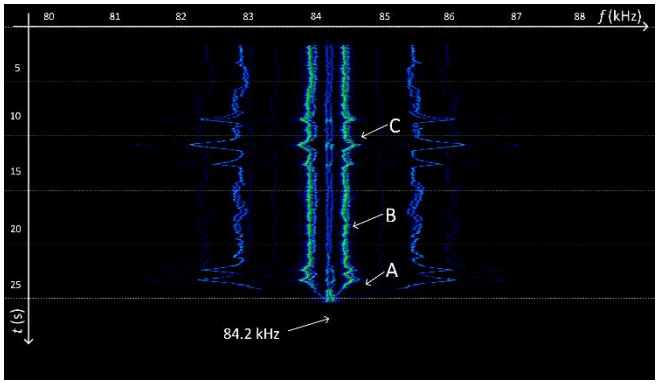


(a)

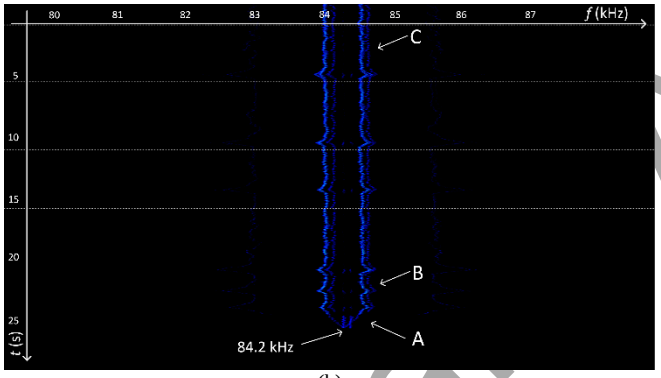


(b)

Fig. 11. DJI AIR 3S electromagnetic signatures of 84.2 kHz at 8-meter distance (a) and at 21-meter (b). The time marks show: A – motors are started; B – drone is in flight stabilisation mode; C – drone is rapidly lifted in vertical axis three times.

The experiment represented in the Fig 11 (a) and (b) is of the same type and procedure as described before except that a different drone was used – the DJI AIR 3S. The EM signature of the drone is of a constant central frequency 84.2 kHz and does not change in the spectrum during all flight modes. The measured distances between the drone and the magnetic antenna are 8 and 21 meters. The results show the same type of signature dependencies as examined during the previous experiment. The main difference is in the amplitude of the visible harmonics and their number. As the higher distance is from drone to the receiving antenna, the lower number and amplitude of visible harmonics are present in the spectrum recorded.

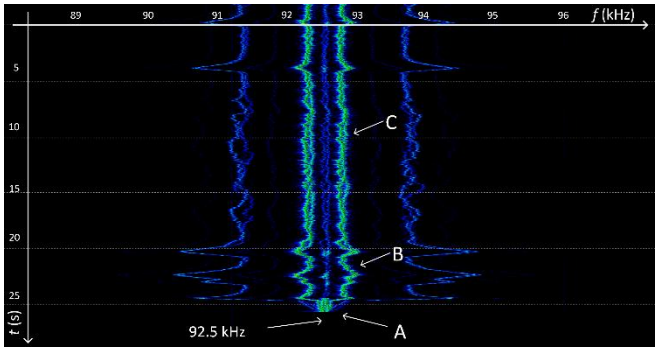


(a)

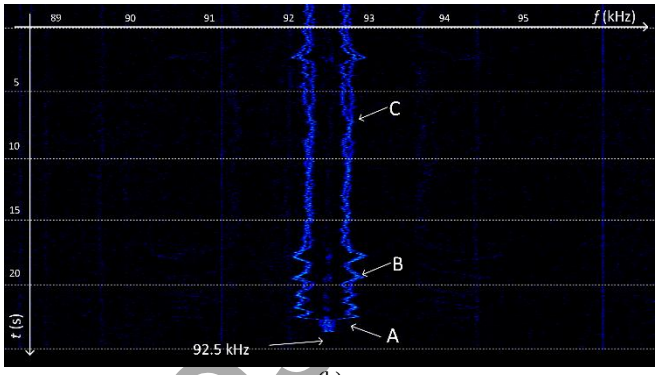


(b)

Fig. 12. EM signatures of the DJI Mavic 2 Enterprise with a center frequency of 92.5 kHz at a distance of 10 meters (a) and 26-meters (b). The time marks show: A – motors are started; B – drone is in flight stabilisation mode; C – drone is rapidly lifted in vertical axis three times.

Fig. 12 (a) and (b) show the spectrograms of the DJI Mavic 2 Enterprise drone test at distances of 10 and 26 meters, respectively. The EM signature of the drone is of a constant central frequency of 92.5 kHz and does not change in the spectrum during all flight modes. The results show the same type of signature dependencies as examined during the previous experiments. The main difference is of the amplitude of the visible harmonics and their number. As the higher distance is from the drone to the receiving antenna, the lower number and amplitude of visible harmonics are present in the spectrum recorded.

The spectrograms in Fig. 13 (a) and (b) show the EACHINE TYRO 109 drone taking off at distances of 13 and 32 meters from the receiving antenna, during the experiment. The flight experiment is performed in the same manner. The EM signature of the drone is constant and does not change in the spectrum at 24.4 kHz PWM switching frequency. The main difference is the amplitude and the number of observed signature widths. As the distance from the receiving antenna to the drone increases, the less the visible harmonics are present in the spectrogram. Also, it should be noted, that the drone is produced by a completely different manufacturer, construction and ESC PWM switching frequency is the lowest in the experimental range. From the spectrograms, it is clear, that drone uses a different approach for the flight stabilisation, as it is minimal for FPV (First-Person View) drone. The recorded vertical permanent lines in the spectrum are artefacts of other received frequencies of the EM sources present in the VLF spectrum.

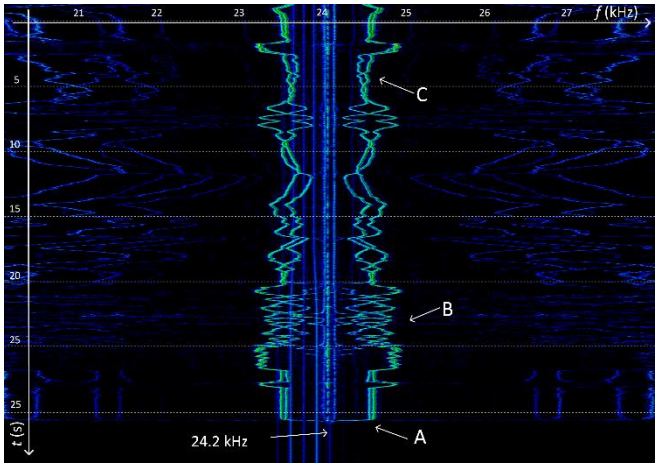


(a)

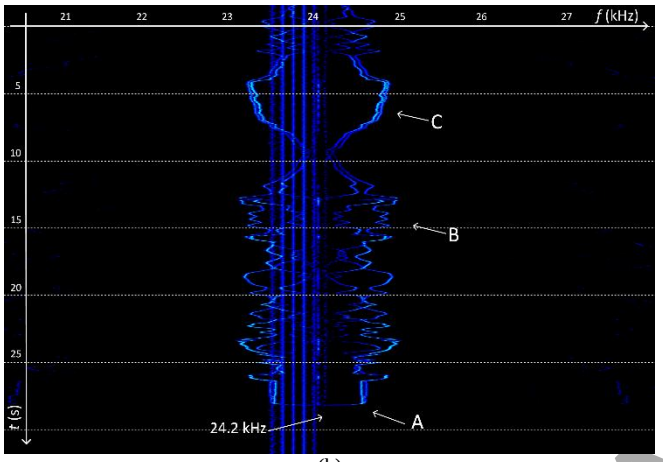


(b)

Fig. 13. Eachine Tyro 109 EM signatures of 24.2 kHz at 13-meter distance (a) and at 32-meter distance (b). The time marks show: A – motors are started; B – drone is rapidly turned to left and right according to its vertical axis; mark C – drone is in flight stabilisation mode.

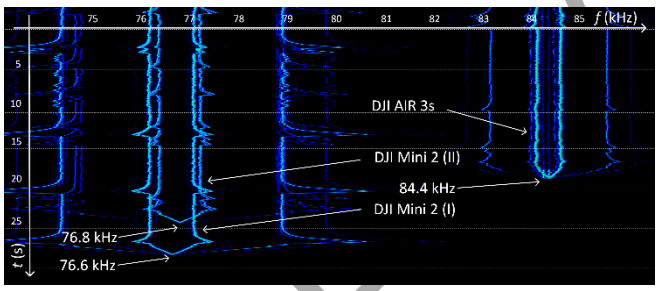


Fig. 14. Three EM signatures of identical serial production drones DJI Mini 2 (I) at 76.6 kHz, DJI Mini 2 (II) at 76.8 kHz and one DJI AIR 3s at 84.4 kHz.

Fig. 14 presents experimental data in a practical case of a drone swarm EM signature detection. In this experiment, three drones were operated simultaneously in the same space under stable air conditions, without gusts of wind or thermal disturbances. Two of the drones were DJI Mini 2 units of the same model and configuration, and the third was a DJI AIR 3s. Although there were two drones of the same model (DJI Mini 2) in flight, the centre frequencies of their EM signatures were slightly different – one was 76.6 kHz, and the other was 76.8 kHz. The central frequency of the EM signature of the third drone (DJI AIR 3s) was completely different – 84.4 kHz. These experimental results clearly demonstrate that same type drones of the same model (signatures DJI Mini 2 (I) and DJI Mini 2 (II)) emit unique and unrepeatable EM signatures that can be received and identified in the spectrum. The difference between the centre frequencies of signatures DJI Mini 2 (I) and DJI Mini 2 (II) is only 200 Hz, but these spectral components can be recognised and highlighted for detection. The third signature of the DJI AIR 3S at 84.4 kHz is also well separated in frequency and thus suitable for analysis and identification. Summarizing the above, the obtained data confirms the feasibility of EM thrust motor signature detection even of drone swarms, including serial production drones of the same model and configuration. Each drone has its own unique aerodynamic and motor construction imperfections, different weight and propeller thrust, which results in visible EM signature change during different flight condition. Each drone generates a characteristic EM signature that can be exploited for detailed examination, recognition, and potentially for tracking individual units within a swarm.

The experiment was performed at least three times with each UAV, and the PWM switching frequency of each UAV remained stable and did not change under any conditions when the thrust motors were powered on. The results in Fig.10, Fig. 11, and Fig. 14 show the three different measurements of the same UAVs, where the centre frequency of PWM switching is the same: for DJI AIR 3s - 84.4 kHz, for DJI Mini 2 (II) - 76,8 kHz. The experiment shows that each UAV has a unique PWM switching frequency, which is observed as a stable EM signature, enabling recognition of individual serially produced UAVs even under swarm flight conditions.

The drone stabilization and flight algorithms control BLDC motor's ESC in different way, which is clearly seen from EM signature in the spectrum. This experiment was performed indoors, without any gusts of wind in stable air conditions, without any thermals, in order to demonstrate the maximally ideal and uniform conditions for every drone under the experiment. In real flight, any introduction of wind, air thermal activity, or flight manoeuvring will result in a more expressed EM signature contributing in UAV recognition. In Fig. 13, vertical permanent lines in the spectrum are artefacts of other received EM emissions at the same frequency as the UAV EM signature. Nevertheless, the UAV EM signature is recognizable.

## IV. DISCUSSION

According to the presented theoretical reasoning about the power structure of drone BLDC motors, a mathematical model and a computer simulation of the quadcopter magnetic field, a drone can be detected by the EM emission of its traction system at a distance of up to 100 m. Computer simulations have shown that at certain points during flight, for a specific combination of amplitudes and phases of the currents powering the BLDC motors and at specific observation angles, the intensity of the magnetic induction generated by the drone is close to zero. However, in real flight conditions, a drone is forced to frequently, if not constantly, perform the function of stabilizing its position in space. As a result, the parameters of the currents supplying the motors are constantly changing, which is the reason that the drone's EM radiation pattern resembles a sphere that is slightly compressed along its equator (the plane of the drone itself) and seems to be "pulsating" without constant zero points of radiation.

The obtained experimental results show that the amplitude of the harmonics and a slight change in frequency around the PWM central frequency exist in the EM signature of drones. The shifts of these harmonics on the frequency axis are directly related to changes in the thrust of the BLDC motors. As the distance from the drone to the antenna increases, the amplitudes of all harmonics of the spectrum decrease and eventually fall below the background noise level. Higher amplitude harmonics produce the EM signature with a change in accordance with thrust motor acceleration and power. The primary signature parameters of the drones under study are presented in Table V.

TABLE V. PRIMARY ELECTROMAGNETIC SIGNATURE PARAMETERS OF INVESTIGATED DRONES.

| Parameter | Drone model | | | |
|---|---|---|---|---|
| | **DJI MINI 2** | **DJI AIR 3S** | **DJI MAVIC 2** | **EACHINE TYRO 109** |
| Maximum distance from the drone when measu-ring the signature (m) | 14 | 21 | 26 | 32 |
| Signature center on the frequency axis (kHz) | 76.8 | 84.2 | 92.5 | 24.2 |
| The width* of the signatu-re when drone is in flight stabilization mode (Hz) | ~800 | ~500 | ~500 | ~700 |
| Maximum measured signature width* (Hz) | ~1600 | ~900 | ~1600 | ~1600 |

*Note: *Signature width* in frequency axis is the difference between the 1st side symmetric harmonics of EM signature.

BLDC electric motors used in drones are typically powered by PWM pulse trains generated by the ESC controller. The PWM switching frequency in this case is within tens, or less often hundreds, of kilohertz, which corresponds to the VLF or LF frequency range. The switching of the ESC power transistors produces characteristic current and voltage waveforms in the stator windings, which in turn generate dynamically changing alternating magnetic fields around the motor, cabling, and battery lines. These fields contain a strong spectral component at the PWM switching frequency and its harmonics, superimposed on the lower-frequency components associated with the frequency of phase commutation of the BLDC motors and, accordingly, with the mechanical rotation of the rotors.

It can also be noted that the EM signatures of some drones obtained during the experiment, for example, the DJI Mini 2, lack a "central" harmonic corresponding to the PWM switching frequency set by the ESC. This fact can be explained by the amplitude symmetry of the current pulses (i.e. changing over time from negative to the same positive amplitude) sent to the BLDC motors. The spectrum of such pulses lacks a DC component and, as a consequence, the EM signature of such a drone does not contain a harmonic corresponding to the PWM switching frequency [7].

The exact spectral content of these emissions depends on the motor parameters (winding configuration, number of pole pairs, magnet material), the ESC topology (phases commutation frequency, dead time, modulation strategy), and the instantaneous operating point (throttle setting, load torque, supply voltage). Small variations in ESC firmware, control loops, or component tolerances can lead to measurable differences in the centre frequency and amplitude of the dominant harmonics between nominally identical BLDC motors. As a result, each motor–ESC combination can exhibit a quasi-unique EM signature, which can be exploited for UAV detection, identification, and classification in the VLF band.

## V. CONCLUSIONS

The theoretical studies presented in the paper and the experiments performed allow us to draw the following conclusions.

1. Electrically powered drones with brushless DC (BLDC) traction motors emit electromagnetic (EM) energy, the frequency spectrum of which is unique and corresponds to a unique EM signature of the drone, by which it can be detected at a distance of up to several tens of meters and recognised.

2. EM drone signature has an acceleration dependency of shifting the frequency value of BLDC motor phase commutation frequency to higher and lower sides from the BLDC motor PWM switching frequency.

3. The experiment results show that different types of drones have a unique PWM switching frequency which can be identified.

4. The absence of a central harmonic in the EM signature of some drones is explained by the amplitude symmetry of the currents supplying their BLDC motors.

5. Even similar drones of the same model produced by the same manufacturer have unique EM signatures, by which they can be detected and recognised among other drones of the same model.

6. Drone swarms can be detected in very low frequency range, as their thrust motor electromagnetic emission signatures can be identified separately.

## APPENDIX A. DRONE PROPULSION MOTOR CONTROL STRUCTURE

In an electrically powered multirotor UAV, the BLDC thrust motors are the mandatory electric propulsion components that convert battery power into motor rotor torque and propeller thrust through electronically controlled three-phase coil commutation [15], [19]. The ESC sequentially energises the stator windings in synchronisation with rotor position, creating a rotating magnetic field that drives the permanent-magnet rotor. Without this commutation process, sustained lift and controlled flight are not possible. PWM is superimposed on the commutation sequence to regulate the effective phase voltage and current, so the PWM duty cycle directly controls electromagnetic torque and, consequently, thrust magnitude. An increase in PWM duty cycle raises the average winding current and propeller loading, while a decrease reduces torque and thrust. For UAV electromagnetic emission detection, this operating principle is fundamental because both the commutation rate and the PWM switching process shape the motor current waveform and therefore generate the measurable VLF and LF spectral components used for EM signature detection [9], [10]. Due to the high torque/weight efficiency BLDC type thrust motors are mandatory and dominant in drone propulsion system design [15]. Their construction and working principles are well known and of minimal change (Fig. A-1).

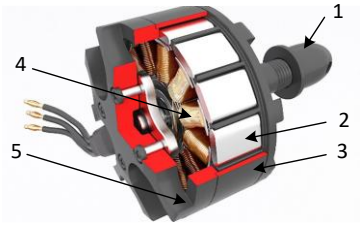


Fig. A-1. Structure of the outrunner type drone BLDC thrust motor; where 1 is the rotating propeller shaft, 2 is the rotating magnets, 3 is the rotor with magnets, 4 is the stationary motor coils, 5 is the stationary motor housing for bearing and coil fixation. Applied from [23].

In BLDC motor propulsion systems, the ESC is used to control each motor thrust independently. The ESC produced BLDC motor control currents do emit EM field change observed in the nearfield region of 1–100 kHz frequency spectrum [14]. The time dependant frequency and amplitude change of the EM signature is influenced not only by drone flight and control parameters, but also by motor design type, drone weight, load, and propeller specifications affecting ESC and flight control microprogram algorithms [15].

The most important BLDC motor construction parameters influencing EM signature are the speed constant Kv, and number of BLDC motor poles. These BLDC motor construction parameters are fixed during the motor manufacture and cannot be changed during the flight. The EM signature is primarily dependant on the PWM switching frequency and BLDC phase commutation time varying currents as it relies on primary motor construction and control characteristics. There are BLDC motors designed for low speed and higher torque, and vice versa, which do have significant differences in ESC commutation produced EM signatures [16].

Multirotor drone flight is achieved through a continuously stabilized, microprocessor-controlled control loop in which the thrust of each BLDC motor is regulated independently. By differentially increasing or decreasing the thrust produced by individual rotors, the flight controller generates the torques required for roll, pitch, and yaw control, while also maintaining stabilized hover, ascent, and descent. In this architecture, every flight mode is directly dependent on the instantaneous thrust of each propulsion unit, which is governed by two coupled ESC control variables: the PWM duty cycle and the motor phase-commutation rate. The commutation sequence determines the timing of phase-current transfer between stator windings, thereby sustaining rotor synchronisation and torque production, whereas the PWM duty cycle regulates the effective phase voltage and current, and thus the produced thrust [18]. Documented BLDC control implementations commonly operate in the range of 4 to 120 kHz, where higher PWM switching frequencies are used for reduced torque ripple or minimising acoustic effects.

This control principle is especially important for UAV electromagnetic signature analysis, because both – the thrust motor coil commutation process and the PWM switching process directly shape the propulsion-current waveform. As a result, the drone's BLDC motor–ESC assembly generates identifiable spectral components at the commutation frequency, the PWM switching frequency, and their harmonics and sidebands.

During UAV flight, the flight controller (Fig. A-2) continuously updates ESC commands based on attitude and thrust demands, causing rapid, motor-specific variations in motor coil commutation rate and PWM switching patterns. These control actions are the primary origin of repeatable electrical (and electromagnetic) signatures: commutation harmonics, PWM carrier components, and load-dependent sidebands tied to propeller thrust and transient manoeuvres.

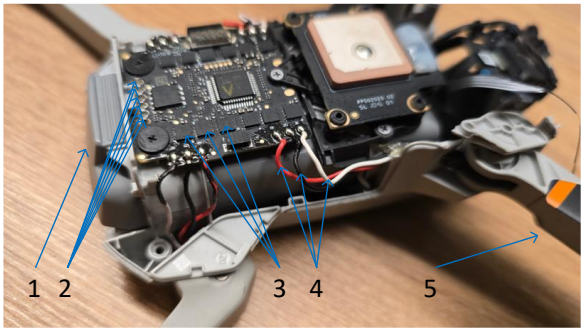


Fig. A-2. DJI Mini 2 ESC board with BLDC power cable connections; where 1 is power battery, 2 is power battery ESC connector, 3 is one of four BLDC motors control transistors, 4 is one of four three phase BLDC motor wires, 5 is one of four folding arms with BLDC thrust motor.

## REFERENCES

[1] U. Seidaliyeva, L. Ilipbayeva, K. Taissariyeva, N. Smailov, and E. T. Matson, "Advances and challenges in drone detection and classification techniques: a state-of-the-art review", *Sensors*, vol. 24, no. 1, pp. 125–155, Dec. 2023. DOI: 10.3390/s24010125.

[2] D. Herath et al., "ELF passive radio sensing and AI-perception of micro-UAS", *IEEE Sensors Journal*, Dec. 15, 2025, Preprints. DOI: 10.1109/JSEN.2026.3665766

[3] D. Aouladhadj et al, "Drone detection and tracking using RF identification signals", *Sensors*, vol. 23, no. 17, pp. 7650–7674, Sep. 2023. DOI: 10.3390/s23177650.

[4] G. De Cubber et al., "Standardized evaluation of counter-drone systems: methods, technologies, and performance metrics", *Drones*, vol. 9, no. 5, pp. 354–379, May 2025. DOI: 10.3390/drones9050354.

[5] K. Yalçin, "Fiber-optic drone technologies: a multidisciplinary review from communication fundamentals to military applications", Jun. 08, 2025, Zenodo. DOI:10.5281/zenodo.15620221.

[6] T. Jačionis and V. Urbanavičius, "Change in the spectrum of EM radiation of the electric propulsion system of a UAV under conditions of forced flight stabilization", in *2024 IEEE 11th Workshop on Advances in Information, Electronic and Electrical Engineering (AIEEE)*, Valmiera, Latvia: IEEE, May, June 2024, pp. 1–6. DOI: 10.1109/AIEEE62837.2024.10586623.

[7] T. Jačionis and V. Urbanavičius, "The influence of brushless thrust motor currents on the electromagnetic drone signature", in *2025 IEEE 12th Workshop on Advances in Information, Electronic and Electrical Engineering (AIEEE)*, Vilnius, Lithuania: IEEE, May 2025, pp. 1–6. DOI:10.1109/AIEEE66149.2025.11050872.

[8] V. Carev, J. Roháč, M. Šipoš, and M. Schmirler, "A multilayer brushless DC motor for heavy lift drones", *Energies*, vol. 14, no. 9, pp. 2504–2523, Apr. 2021. DOI:10.3390/en14092504. DOI: 10.3390/en14092504.

[9] I. Bodnar, R. R. Boros, D. Erdosy, and D. Matusz-Kalasz, "Electromagnetic emission of BLDC motor controllers", in *2021 22nd International Carpathian Control Conference (ICCC)*, Velké Karlovice, Czech Republic: IEEE, May 2021, pp. 1–6. DOI: 10.1109/ICCC51557.2021.9454655.

[10] *Nomenclature of the frequency and wavelength bands used in telecommunications*, Recommendation ITU-R V.431-9, International Telecommunication Union, 10/2025. Available at: www.itu.int/publ/R-REC/en.

[11] R. Barr, D. L. Jones, and C. J. Rodger, "ELF and VLF radio waves", *Journal of Atmospheric and Solar-Terrestrial Physics*, vol. 62, no. 17–18, pp. 1689–1718, Nov. 2000. DOI: 10.1016/S1364-6826(00)00121-8.

[12] J. De La Cruz Soto et al., "Analysis and assessment of a brushless DC outrunner motor for agriculture drones using JMAG", *Applied System Innovation*, vol. 8, no. 3, pp. 81–107, Jun. 2025. DOI: 10.3390/asi8030081.

[13] H. A. Hashim, "Advances in UAV avionics systems architecture, classification and integration: a comprehensive review and future perspectives", *Results in Engineering*, vol. 25, pp. 103786–103804, Mar. 2025. DOI: 10.1016/j.rineng.2024.103786.

[14] J. Blažek, P. Lipovský, F. Heško, and D. Repčík, "Electromagnetic image of small UAV in very low frequency range", *Journal of Electrical Engineering*, vol. 69, no. 6, pp. 438–441, Dec. 2018. DOI:10.2478/jee-2018-0069.

[15] O. Solomon and P. Famouri, "Dynamic performance of a permanent magnet brushless DC motor for UAV electric propulsion system – Part I", in *IECON 2006 – 32nd Annual Conference on IEEE Industrial Electronics*, Paris, France: IEEE, Nov. 2006, pp. 1400–1405. DOI: 10.1109/IECON.2006.347808.

[16] D. Mohanraj et al., "A review of BLDC motor: state of art, advanced control techniques, and applications", *IEEE Access*, vol. 10, pp. 54833–54869, 2022. DOI: 10.1109/ACCESS.2022.3175011.

[17] M. P. Stewart, S. T. Martin, "Unmanned aerial vehicles: fundamentals, components, mechanics, and regulations", in book: *Robotics Research and Technology*, New York, Nova Science Publishers, Incorporated, pp. 1–70, 2021, ch. 1.

[18] K. P. Valavanis and G. J. Vachtsevanos, Eds, *Handbook of Unmanned Aerial Vehicles*. Dordrecht: Springer Netherlands, 2015.

[19] T. Kenjō, S. Nagamori, T. Kenjō, S. Nagamori, and T. Kenjō, "Permanent-magnet and brushless DC Motors" in *Monographs in electrical and electronic engineering*, no. 18. Oxford: Clarendon Pr, 1985.

[20] Z. Vainoris, *Fundamentals of Wave Electronics* (in Lithuanian). Vilnius, Technika, 2004, pp. 369–372.

[21] J. D. Kraus and R. J. Marhefka, *Antennas. For All Aplications.* McGraw-Hill Higher Education, 2001, pp. 726–729.

[22] R. D. Straw (Ed.), L. B. Cebik, D. Hallidy, D. Jansson, R. Lewallen, *The ARRL antenna book: The ultimate reference for amateur radio antennas, transmission lines and propagation*, 21st ed. Newington, Conn: ARRL, 2007.

[23] *Electric Motor RC Inside*, Free3D© models. Available at: https://free3d.com/3d-model/electric-motor-rc-inside-20-4085.html?dd_referrer=https%3A%2F%2Fwww.google.com%2F